Effect of Bulk Miscibility on the Surface Composition of Polypropylene/ Poly(ethylene-*co*-propylene) Blends

Aric Opdahl,[†] Roger A. Phillips,[‡] and Gabor A. Somorjai*[,†]

Department of Chemistry, University of California at Berkeley and Materials Science Division, Lawrence Berkeley National Laboratory, Berkeley, California 94720, and Research & Development Center, Basell USA Incorporated, 912 Appleton Road, Elkton, Maryland 21921

Received October 12, 2001

ABSTRACT: The surface composition profiles of bulk miscible and immiscible blends of atactic polypropylene (*a*PP) with aspecific poly(ethylene-*co*-propylene) rubber (*a*EPR) were studied by differential scanning calorimetry (DSC), sum frequency generation surface vibrational spectroscopy (SFG), and X-ray photoelectron spectroscopy (XPS). SFG spectra of blends of *a*PP and *a*EPR show that *a*PP preferentially segregates to the air/polymer interface, for both the bulk miscible and immiscible systems. The SFG spectra also indicate that methyl side branches assume a preferred configuration at the air/polymer interface, which may play a role in the high surface activity of *a*PP. Bulk miscibility is shown to control the thickness of the surface enrichment layer, with thicker enrichment layers detected by XPS on bulk immiscible blends. The thickness of the surface enrichment layer measured in the bulk miscible systems is in agreement with the thickness calculated using existing depth profiling models based on Flory−Huggins energy of mixing.

Introduction

The surface and bulk phase behavior of polyolefin copolymers and blends has received considerable attention in recent years in large part because of their continued commercial importance. Polyolefin synthesis also enables the careful control of architectural variables, such as short-chain branching and tacticity, with similar hydrophobic units. This control has led to the use of polyolefins as model systems for studying the underlying molecular phenomena governing the fundamental properties of polymers including surface segregation and bulk phase behavior.

Many experimental[1−3] and theoretical[4−7] studies have been made in an attempt to better understand surface segregation in polyolefin blends. Recently, side branches have been found to be a key variable in determining the surface activity of polyolefins. Depth profiling measurements have shown that, for blends of polyolefin copolymers with different number densities of ethyl side branches, the more branched copolymer has a tendency to segregate to the air/polymer interface.[1,2] In the cases involving polyolefin blends and also cases involving blends of polystyrene and deuterated polystyrene,[2,8−10] the theory developed by Schmidt and Binder[4] which incorporates the Flory−Huggins interaction parameter, χ_{ab}, and the difference in surface chemical potential of the blend components has been applied to describe the shape of experimentally measured depth profiles.

For miscible and partially miscible blends, it is generally accepted that the enthalpic cohesive energy of the individual components plays a large role in determining the surface composition at the air−polymer interface, with the component having the lowest cohesive energy, or surface tension, being favored at that interface. The extent that entropy controls the surface conformation is less understood.[3,5] Theoretical results suggest that conformational entropy, related to the size of the random coil, and packing entropy related to the configuration of the polymer at the interface play competing roles in mixtures of branched polyolefins at the air interface.

Our recent sum frequency generation (SFG) vibrational spectroscopy investigations of polyolefin surfaces have shown that, at the molecular level, many polyolefins assume specific conformations at the air interface.[11−13] In particular, aspecific poly(ethylene-*co*-propylene) copolymers (*a*EPR) synthesized with varying number densities of methyl side branches have been shown to configure themselves in a way that preferentially orients the methyl side branch away from the bulk at the air/polymer interface.[13] Additionally, the sum frequency results indicate that chain backbones tend to lie parallel to the surface plane, with ethylene-rich polymer backbones having a stronger tendency to lie in the surface plane. These specific types of molecular interactions at the air/polymer interface, measured for the pure components, may also affect the surface segregation properties for blends of *a*EPR copolymers.

The segregation thermodynamics for bulk immiscible polymers are not as well understood as the miscible case. At the surface, a wetting transition from complete to partial wetting has been predicted for the immiscible case and is predicted to be dependent on the degree of immiscibility as well as the difference in surface activities of the blend components.[14] This transition to partial wetting is expected to occur by lowering the temperature of the blend far below the critical temperature, increasing the molecular weight of the blend components, or decreasing the relative surface affinities of the blend components.

In this study, sum frequency generation surface vibrational spectroscopy (SFG), X-ray photoelectron spectroscopy (XPS), and differential scanning calorimetry (DSC) have been used to examine the surface molecular structure, the chemical morphology of the

[†] University of California at Berkeley.
[‡] Basell USA Incorporated.
* Corresponding author: fax 510-643-9665; e-mail somorjai@socrates.berkeley.edu.

10.1021/ma011773q CCC: $22.00
Published on Web 04/17/2002

Table 1. Structural Characteristics of the *a*EPR Copolymers

sample	M_w	M_w/M_n	wt % ethylene	mol % ethylene	$[CH_2]/[CH_3]_{bulk}$	sequence parameter[b]
*a*PP1[a]	54 000	2.0	0	0	1	
*a*PP2[a]	210 000	2.0	0	0	1	
*a*EPR2	48 000	2.0	4.7	6.9	1.15	1.0
*a*EPR3	54 000	2.0	7.1	10.3	1.23	1.0
*a*EPR4	54 000	2.0	13.5	19.0	1.47	1.1
*a*EPR5	48 000	2.1	20.3	27.7	1.76	1.3
*a*EPR6	54 000	2.0	25.9	34.4	2.05	1.3
*a*EPR7	54 000	1.9	32.3	41.7	2.43	1.4

[a] 16% iso triads, 49%hetero triads, 35%syndio triads. [b] The sequence parameter, determined by NMR, is a measure of the randomness of the copolymer. It is 1 for a completely *random* distribution of comonomers, 2 for complete *alternation* of comonomers, and 0 for complete *block*like sequencing.

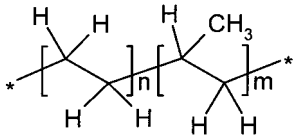

Figure 1. Structure of aspecific poly(ethylene-*co*-propylene) rubber (*a*EPR). The distribution of block lengths (*n, m*) is very nearly random, and methyl group placement in the propylene units lacks stereospecificity.

surface region, and the bulk phase behavior of miscible and immiscible blends of atactic polypropylene (*a*PP) with aspecific poly(ethylene-*co*-propylene) rubber (*a*EPR). Each of the blend components has the basic structure given in Figure 1 and is comprised of similar CH_2 and CH_3 units. Blend miscibility is controlled by varying the molecular weight of the *a*PP component.

These model blends mimic the important commercial blend of isotactic PP/EPR, without complications due to crystallinity, through the use of an aspecific polymerization catalyst. SFG and XPS are both surface-sensitive techniques and can distinguish between the CH_3 unit in propylene and the CH_2 unit, which is present in both the ethylene and propylene repeat units.[13,15] Additionally, SFG and XPS, applied to *a*PP/*a*EPR blends, do not require isotopic labeling, and because SFG is a photon-based technique and XPS is an electron-based technique, each technique is sensitive to a different depth of the surface and gives a different type of chemical information.

SFG is a second-order nonlinear optical technique that, in the absence of bulk ordering, is specifically sensitive to the molecular composition and orientation of the surface monolayer. XPS is based on the detection of photoelectrons. The surface sensitivity of XPS is limited by the mean free path of those photoelectrons in the polymer film and is typically a few nanometers. The depth of sampling can be controlled to some extent by varying the detection angle with respect to the surface plane. Thus, SFG can be used to determine the composition of the surface monolayer, while XPS can be used to integrate the chemical composition of the top few nanometers of the surface. Because SFG is specifically sensitive to the conformation of the polymer units at the interface, we are also able to deduce differences in interfacial packing of the individual blend components. SFG spectra of *a*PP/*a*EPR blends show that *a*PP, the component with the larger number of methyl side branches, preferentially segregates to the air/polymer interface for both the bulk miscible and bulk immiscible blends. The thickness of the *a*PP enrichment layer is detected by XPS and is shown to increase for the bulk immiscible blend.

Experimental Section

Polymers. Table 1 summarizes the samples used in this study, which have the generalized structure depicted in Figure 1. The results in Table 1 indicate that the distribution of block lengths (*n, m*) in Figure 1 is very nearly random and that methyl group placement in the propylene units lacks stereospecificity. Dibutylsilylbis(9-fluorenyl)zirconium dichloride catalyst was used to prepare the atactic polypropylene homopolymers (*a*PP1 and *a*PP2) and aspecific ethylene/propylene copolymer/rubber (*a*EPR2-7) in hexane with a methylaluminoxane (MAO) activator at 70 °C polymerization temperature and a molar [Al]/[Zr] ratio of 2000−3000. Closely related analogues to this aspecific catalyst have been published previously.[16] The *a*PP homopolymers, *a*PP1 and *a*PP2, differ only in their molecular weight. The ethylene/propylene copolymers differ in their ethylene content—*a*EPR7 has the highest ethylene content (32.3 wt %). The *a*EPR copolymers were prepared by maintaining a constant monomer feed ratio. DSC analysis of each of the copolymers showed single composition dependent glass transition temperatures with no evidence of crystallinity. The higher molecular weight *a*PP homopolymer (*a*PP2) was prepared at lower polymerization temperature (50 °C). The polymers were dissolved in hexane solutions, filtered to remove larger-scale polymerization impurities, and recovered by evaporation of solvent.

Tacticity and composition of each homopolymer were determined by ^{13}C NMR using a Varian UNITY-300 spectrometer at 75.4 MHz in 10% *o*-dichlorobenzene solutions at 130 °C. Ethylene content was determined from the compositional triads. The NMR sequence parameter (s.p.), determined from compositional diads, is given in Table 1 and has a value of 1 for a random distribution of comonomers, is >1 for alternating sequencing (s.p. = 2 for complete alternation), and <1 for blocklike sequencing (s.p. = 0 for complete blocks).[17] The weight-average molecular weight (M_w) and polydispersity (M_w/M_n) were determined by high-temperature gel permeation chromatography in trichlorobenzene using a Waters 150-C GPC calibrated with polystyrene standards and converted to PP equivalents without further correction for ethylene content.

Solutions containing 5 wt % polymer were prepared in *n*-hexane and allowed to equilibrate for at least 2 days. The primary blend systems were blends of *a*PP1 and *a*EPR7 and blends of *a*PP2 and *a*EPR7. Blends were prepared by mixing appropriate amounts of each solution and were allowed to equilibrate for an additional 2 days. Thin films for SFG and XPS analysis were prepared by spin-casting solutions onto IR grade fused silica substrates. After casting, the films were annealed at 70 °C for 12 h. Films were measured by atomic force microscopy to have thickness between 200 and 300 nm. Both SFG and XPS measurements were made at room temperature, above the glass transition temperature of each of the blend components.

Differential Scanning Calorimetry (DSC). Samples for differential scanning calorimetry (DSC) were prepared by dissolving 0.5 g of polymer (*a*PP, *a*EPR, or *a*PP/*a*EPR blend) in 15 mL of hexane or heptane for at least 24 h and then filtering through 5 μm filters into Teflon casting dishes. Films were recovered after solvent evaporation, vacuum-dried atroom

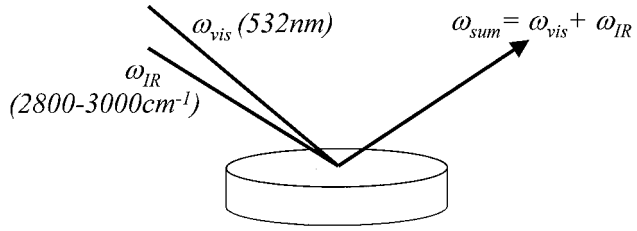

Figure 2. Schematic of SFG beam geometry showing input beams (ω_{vis} and ω_{ir}) overlapping at the surface of the polymer film and the induced sum frequency beam (ω_{sum}).

temperature overnight, and stored in a cold room prior to DSC analysis. Baseline subtracted DSC scans were performed from −110 to 120 °C at 20 °C/min in a Perkin-Elmer DSC-7 calorimeter with liquid nitrogen cooling and helium purge using 15 mg samples taken from the as-cast films. Additional experiments applied a melt cycle by heating (20 °C/min) the as-cast films to 200 °C for 2 min, quenching (320 °C/min) to −110 °C for 10 min, and reheating (20 °C/min). The as-cast films were also annealed at various temperatures by sealing the samples in DSC pans and placing the pans in sealed vials and annealing in a thermostated oil bath for 16 h at temperatures ranging from 50 to 150 °C. The annealed samples were characterized by DSC in an identical manner as the as-cast films.

Sum Frequency Generation Vibrational Spectroscopy (SFG). Surface vibrational spectra were obtained by sum frequency generation (SFG) vibrational spectroscopy. Briefly, surface vibrational spectra of the polymers were collected using the geometry shown in Figure 2 where a visible and a tunable infrared laser beam are overlapped on the surface at incident angles of 50° and 55°, and the induced sum-frequency signal is measured in the reflected direction. The visible beam (ω_{VIS}) is 532 nm light generated by frequency-doubling the 1064 nm fundamental output from a Continuum YAG-PY61 laser (generating ∼20 ps pulses at 20 Hz and 35 mJ/pulse) through a KTP crystal. The tunable infrared beam (ω_{IR}) is generated from a LaserVision OPG/OPA (optical parametric generation)/(optical parametric amplification) system composed of two counter-rotating KTP crystals driven by a portion of the 532 nm light. The idler output of the OPG/OPA stage is mixed with some of the fundamental 1064 nm light in a difference frequency mixing stage composed of two counter-rotating KTA crystals to generate an IR source tunable from 2000 to 4000 cm^{-1}. Surface vibrational spectra were obtained by tuning the infrared beam and measuring the sum-frequency signal as a function of the infrared frequency. The sum-frequency output signal ($\omega_{sum} = \omega_{vis} + \omega_{ir}$) was collected by a gated integrator and photon counting system.

Many additional details are available in recent reviews.[18,19] In general, the measured sum frequency signal is proportional to the square of the second-order nonlinear susceptibility of the excited medium, $\chi^{(2)}$ (eq 1). For vibrationally resonant SFG, $\chi^{(2)}$ is divided into two components, a nonresonant term (χ_{NR}) and a resonant term, where the resonant term is assumed to have a Lorenztian line shape. Resonant enhancement occurs when the infrared source (ω_{IR}) is tuned near a vibrational mode (ω_q). Here A_q is the vibrational mode strength, and Γ_q is the damping coefficient for a particular mode, q.

$$I(\omega_{sum}) \propto |\chi^{(2)}|^2 = |\chi_{NR} + \sum_q \frac{A_q}{\omega_{IR} - \omega_q + i\Gamma_q}|^2 \qquad (1)$$

A_q is related to the molecular hyperpolarizabilty, β_q, in eq 2 by the number density of contributing molecules, n, and an orientation averaged coordinate transformation between the lab-fixed (I,J,K) and molecule-fixed (i,j,k) coordinates.

$$A_{q,IJK} = n\sum_{ijk}\langle\beta_{q,ijk}\rangle \qquad (2)$$

The molecular hyperpolarizability is interpreted in eq 3 as the product of the polarizability (dα/dQ) and dipole (dμ/dQ) derivatives and gives the constraint that the vibrational mode must be both IR- and Raman-active for a sum frequency signal to be resonantly enhanced. This constraint leads to the selection rule that only species lacking inversion symmetry contribute to the sum frequency signal. For bulk isotropic materials, inversion symmetry is broken if the interfacial molecules exhibit polar ordering, and a sum frequency signal can be generated from those interfacial molecules.

$$\beta_{q,ijk} \propto \frac{d\alpha_{ij}}{dQ}\frac{d\mu_k}{dQ} \qquad (3)$$

Spectra were collected using the $s_{sum}s_{vis}p_{ir}$ polarization combination which probes the yyz component of A_q. This polarization combination is most sensitive to vibrations that have a component of the vibrational dipole (μ_k) along the surface normal, z, and a component of the polarizability tensor (α_{ij}) in the surface plane ($x-y$). Experimental data have been fit to eq 1 in order to extract values for $\boldsymbol{A}_q$ for each vibrational resonance.

X-ray Photoelectron Spectroscopy (XPS). XPS experiments were performed on a Perkin-Elmer PHI 5300 XPS spectrometer with a position-sensitive detector and a hemispherical electron energy analyzer. The Mg Kα X-ray emission (1253.6 eV) was used as the probe and was generated with 400 W (15 kV acceleration voltage) at the Mg cathode. A pass energy of 178 eV was used for survey spectra with a 45° takeoff angle, and a pass energy of 35 eV was used for spectra of the valence band region at a 45° takeoff angle. The sampling depth of the XPS experiments is based on an attenuation length of 2.9 ± 0.4 nm measured by Roberts et al. for photoelectrons ejected from PMMA having a kinetic energy of 1200 eV.[20] Using this value as an approximation for the attenuation length of valence band photoelectrons generated by the Kα X-ray source (kinetic energy of photoelectrons ∼1240 eV) leads to a 95% sampling depth of 6.1 ± 0.8 nm.[21]

Results

Bulk Phase Behavior. Figure 3a shows DSC scans of films of low molecular weight polypropylene (*a*PP1), the ethylene/propylene copolymer with the highest ethylene content (*a*EPR7), and a 50:50 wt % *a*PP1/*a*EPR7 blend of the two components cast from heptane. Figure 3a shows that the 50:50 blend has a single glass transition temperature (T_g) at −30 °C, intermediate between the *a*PP1 (T_g 0 °C) and *a*EPR7 (T_g −46 °C) components. The breadth of the transition region is greater in the blend than the individual components. This behavior is typical of a miscible blend and indicates that blends of low molecular weight *a*PP1 and *a*EPR7 solution cast from heptane (or solvents with increased volatility) are in a single miscible phase as measured by glass transition measurements. The *a*PP1 and *a*EPR7 components will be in a single phase at room temperature for all blend compositions, since the 50:50 wt % blends are very near the critical composition, which will have the strongest tendency for phase separation.

Figure 3b shows DSC scans of films of the 50:50 wt % low molecular weight *a*PP1/*a*EPR7 blend as a function of annealing temperature (16 h anneal period). There is possibly a very weak splitting of the T_g-region (most evident for films annealed at 100 and 125 °C), although the inflections in the curves are very slight and far removed from the transitions for the individual *a*PP1 and *a*EPR7 components seen in Figure 3a. This indicates that any phase separation which may occur is very weak.

In contrast to Figure 3a, Figure 3c shows DSC scans of as-cast films (from hexane) of high molecular weight

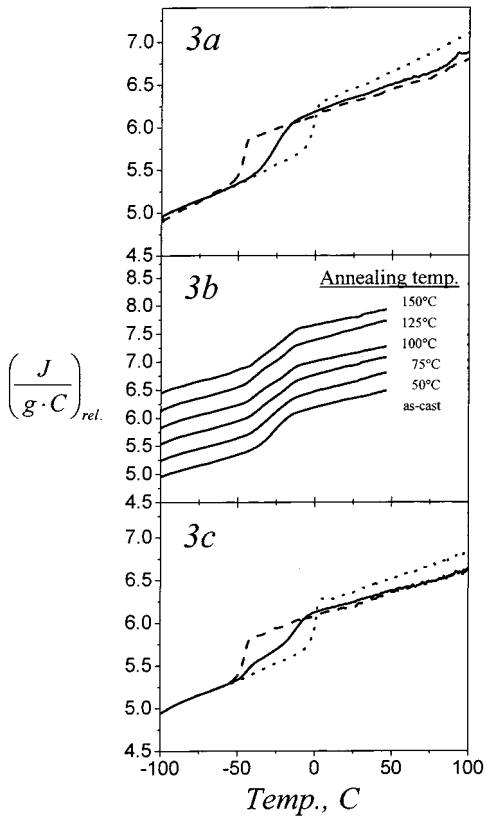

Figure 3. DSC scans (20 °C/min) of individual components and blends: (a) DSC scans of *a*PP1 (dotted), *a*EPR7 (dashed), and 50:50 wt % *a*PP1/*a*EPR7 blend (solid). The blend shows a single phase transition intermediate to the individual components, indicating that the blend is in a single miscible phase. (b) DSC scans of 50:50 wt % *a*PP1/*a*EPR7 blends following annealing at various temperatures, showing the stability of the single phase (scans are vertically offset for clarity of presentation). (c) DSC scans of *a*PP2 (dotted), *a*EPR7 (dashed), and 50:50 wt % *a*PP2/*a*EPR7 blend (solid). This blend shows a split phase transition, indicating that this blend is not bulk miscible.

polypropylene (*a*PP2), the ethylene/propylene copolymer with the highest ethylene content (*a*EPR7), and a 50:50 wt % *a*PP2/*a*EPR7 blend of the two components. The *a*PP2 sample has the same tacticity microstructure as *a*PP1 but with higher molecular weight (Table 1). Two T_g's are visible on the DSC trace of the blend, showing clear phase separation of the *a*EPR7 and *a*PP2 components. Although not shown, phase separation is stable to a melt cycle (see Experimental Section), where the individual T_g's in the blend become sharper. This observation is consistent with an immiscible melt in the 50:50 wt % *a*PP2/*a*EPR7 blend. The blend T_g's are shifted somewhat relative to the parent polymers, most prominently for the *a*PP2-rich phase.

Surface Monolayer Composition of Pure Components and Blends. *SFG Spectra of Poly(ethylene-co-propylene) Rubber Series.* Surface monolayer compositions and configurations were characterized by SFG. The *a*EPR copolymers of varying bulk composition were used as a calibration series for estimating the surface composition of the blends. Because the *a*EPR copolymers are nearly random in nature, macroscopic surface segregation of long sequences of ethylene or propylene in the copolymer backbone is not expected to play a role in the surface segregation behavior. SFG spectra collected using the ssp polarization combination of *a*PP1, *a*EPR4, and *a*EPR7 are shown in Figure 4. The *a*PP1

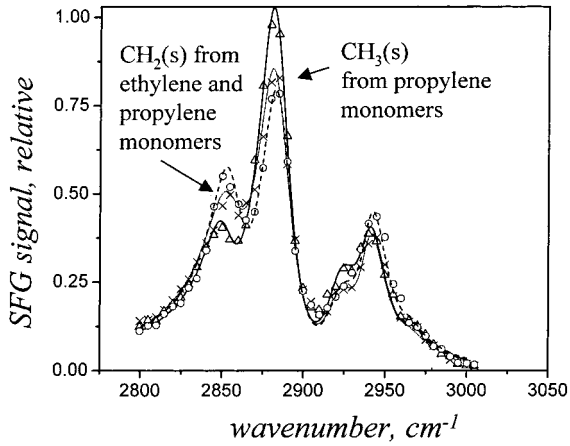

Figure 4. SFG spectra of *a*PP1 (△), *a*EPR5 (×), and *a*EPR7 (○) ssp polarization combination. Solid lines represent the best fit to eq 1.

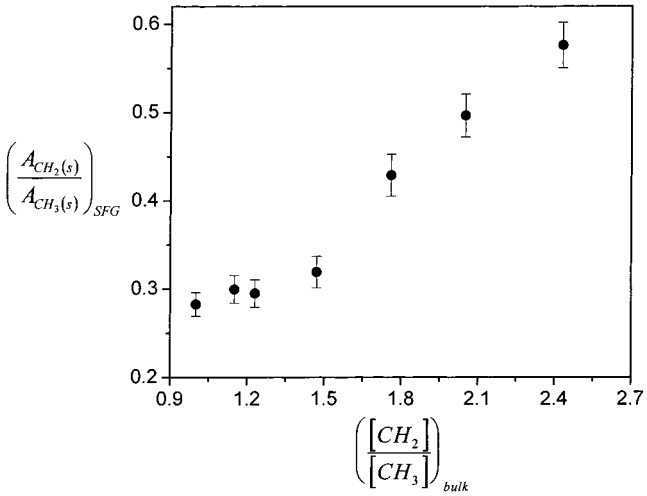

Figure 5. CH_2(s)/CH_3(s) SFG vibrational mode strength (A_q) ratio vs bulk [CH_2]/[CH_3] composition for *a*PP1 and the *a*EPR copolymer series. Vibrational mode strengths are related to the SFG signal intensity through eq 1.

spectra are similar to previously published spectra where the features at 2883 cm^{-1} and the weak shoulder at 2965 cm^{-1} are assigned as the CH_3 symmetric and antisymmetric stretches, respectively.[11] The features at 2850 and 2920 cm^{-1} are assigned as the CH_2 symmetric and antisymmetric stretches, respectively, from the CH_2 backbone. An additional feature at 2940 cm^{-1} arises from the Fermi resonance between the CH_3(s) mode and an overtone of the CH_3 bending mode.

The *a*EPR spectra contain the same features as *a*PP1; however, the peak attributed to the CH_2(s) stretch becomes larger relative to the methyl symmetric stretch as the ethylene content increases. Each of the spectra can be fit to eq 1 using five peaks where A_q is the mode strength, ω_q is the position of the vibrational peak, and Γ_q is the damping factor for the vibration.

The ratio of the fitted mode strengths, A_q, of the methylene CH_2(s) stretch (2855 cm^{-1}) to the methyl CH_3(s) stretch (2883 cm^{-1}) as a function of bulk composition for the *a*EPR series is shown in Figure 5. The dependence is roughly linear over the concentration range we have investigated, qualitatively consistent with the changes in bulk composition. However, because the SFG mode strengths represent a convolution of concentration and orientation (eq 3), the trend in the

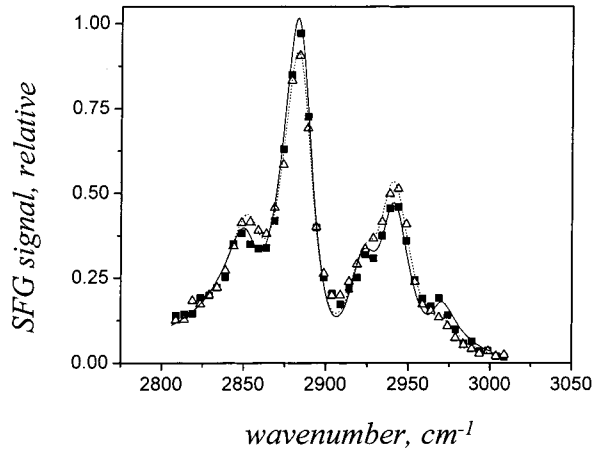

Figure 6. SFG spectra of an "as-cast" 50:50 wt % *a*PP1/*a*EPR7 blend (△) and 50:50 wt % *a*PP2/*a*EPR7 blend annealed for 15 h at 50 °C (■). ssp polarization combination. Solid lines represent the best fit to eq 1.

mode strength ratio does not reflect only the changes in composition, but more accurately the mode strength ratio reflects changes in the total configuration of each of the polymers at the interface.

The detailed analysis of the *a*PP and *a*EPR SFG spectra, separating the orientation effects from the compositional changes, was the focus of another paper.[13] Those results suggest that the ratio between the CH_2-(s) and CH_3(s) mode strengths is related to significant differences in orientation of the polymer backbone between *a*PP1 and *a*EPR7 at the surface. Both *a*PP1 and the *a*EPR7 copolymer tend to preferentially order pendant methyl groups out of the surface at the air/polymer interface. Qualitatively, this is evident by the large CH_3(s) peak for both the *a*PP and the *a*EPR7 spectra shown in Figure 4. The tendency to extend bulky hydrophobic side branches into the air or vacuum is an effect that has been observed both experimentally[22−24] and theoretically[25,26] for several different polymers. Quantitatively, it was determined that *a*EPR7 orients fewer methyl groups per unit surface area compared to *a*PP1. After taking into account differences in the bulk concentrations of methyl groups, however, *a*EPR7 was found to orient a large surface excess (∼40%) of methyl groups relative to *a*PP1. The "excess" of oriented methyl groups is thought to be a result of decreased steric hindrances between neighboring methyl groups in the ethylene-rich copolymer. Additionally, it was deduced that *a*EPR7 is likely to exist in longer sequences of trans oriented backbone segments at the surface than *a*PP1.

Although the ratio of the CH_2(s) to CH_3(s) mode strengths reflects differences in chain configuration, the ratio of the CH_2(s) to CH_3(s) mode strengths is used in this analysis as an indicator of the surface composition. Under the assumption that in a blend of aPP and aEPR7 the surface configurations of the individual components do not change significantly, a high value of the CH_2(s)/CH_3(s) mode strength ratio denotes an *a*EPR7-rich surface whereas a low value denotes an *a*PP-rich surface.

Blend Systems. Figure 6 shows the SFG spectra taken from a 50:50 wt % bulk miscible *a*PP1/*a*EPR7 blend film within the first 2 h after spin-casting from *n*-hexane. Figure 6 also shows the SFG spectra taken from an identical film after it was annealed for 15 h at 50 °C. The CH_2(s) and CH_3(s) features present in the spectra of the as-cast film are intermediate to the CH_2(s) and

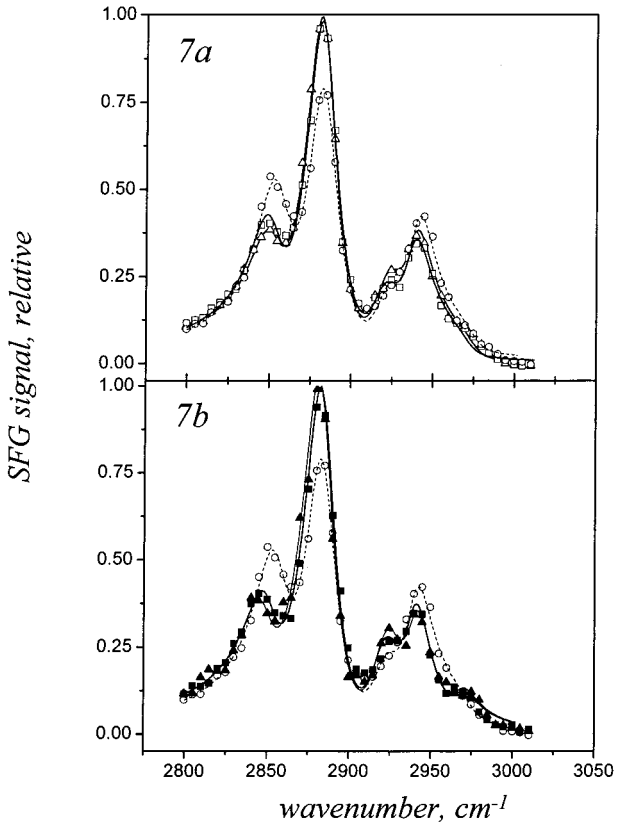

Figure 7. (a) SFG spectra of *a*PP1 (△), *a*EPR7 (○), and 50:50 wt % *a*PP1/*a*EPR7 blend (□). (b) SFG spectra of *a*PP2 (▲), *a*EPR7 (○), and 50:50 wt % *a*PP2/*a*EPR7 blend (■). ssp polarization combination. Solid lines represent the best fit to eq 1.

CH_3(s) features of *a*PP1 and *a*EPR7 presented in Figure 4. This is an indication that, immediately after casting the blend film, both components of the blend are present at the surface and that segregation due to effects of the solvent evaporation is not a major concern.

After the annealing process, the CH_2(s) peak decreases and the CH_3(s) peak increases in magnitude. This shows that the blend film was not in its equilibrium state after it was spin-cast. SFG spectra collected after an additional 15 h 50 °C annealing period and a third set collected 3 weeks later after a final 15 h annealing period at 50 °C yielded indistinguishable results, indicating that after the initial 15 h anneal an equilibrium surface coverage had been reached.

The CH_2(s) and CH_3(s) features of the annealed film are much more "*a*PP1-like" than the as-cast blend, showing that there is a preference for *a*PP1 to segregate to the surface. SFG spectra of low molecular weight *a*PP1, *a*EPR7, and a 50:50 wt % *a*PP1/*a*EPR7 blend sample annealed at 50 °C for 15 h are shown in Figure 7. Qualitatively, the spectra for the 50:50 *a*PP1/*a*EPR7 blend is nearly identical to the *a*PP1 spectra, indicating preferential segregation of *a*PP1 to the surface. The ratios of the CH_2(s) mode strength to the CH_3(s) mode strength for the annealed 50:50 wt % blend and other blend compositions, an *a*PP1-rich 85:15 wt % and an *a*EPR7-rich 15:85 wt % blend, are plotted in Figure 8 along with the ratios for the *a*EPR calibration series. For the 50:50 blend and for the 85:15 *a*PP1-rich compositional blend, the ratio of the CH_2(s) mode strength to CH_3(s) mode strength is, within our experimental uncertainty, identical to the ratio for *a*PP ([CH_2]/[CH_3]

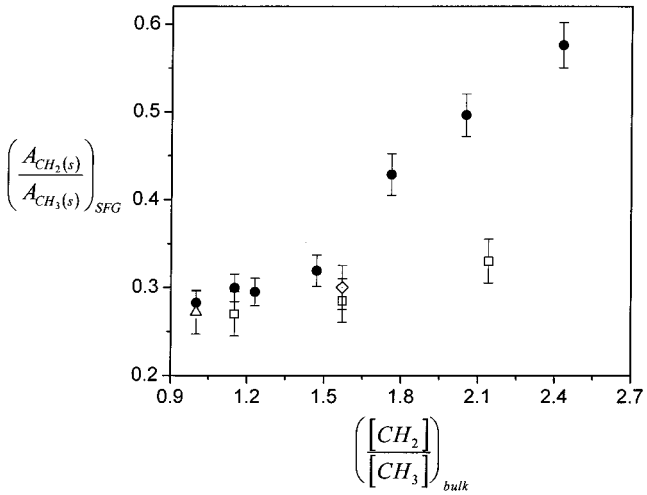

Figure 8. $CH_2(s)/CH_3(s)$ SFG vibrational mode strength ratio (A_q) vs bulk $[CH_2]/[CH_3]$ composition for *a*PP1 and the *a*EPR copolymer series (●), *a*PP1/*a*EPR7 blends (□), *a*PP2 (△), and *a*PP2/*a*EPR7 blends (dotted ◇). All of the blends show a low mode strength ratio relative to the calibration series, indicating that the surface monolayer is enriched in polypropylene.

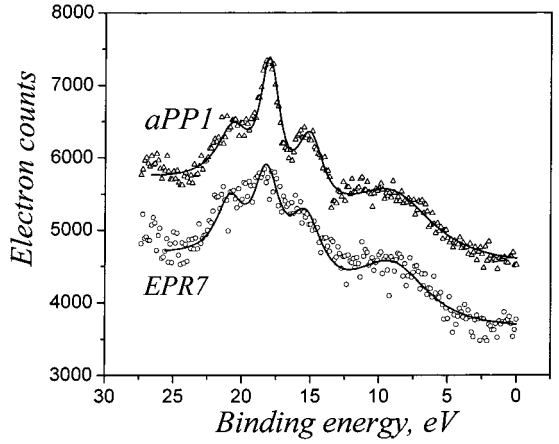

Figure 9. Valence XPS spectra of *a*PP1 and *a*EPR7. Spectra are vertically offset for clarity of presentation. Solid lines represent the best-fit results. The ratio of the CH_2 peaks at 15 and 21 eV to the CH_3 peak at 18 eV increases as the ethylene content of the copolymer increases.

= 1), indicating a large surface excess of *a*PP. For the *a*EPR7-rich 15:85 blend, the mode strength ratio is slightly higher than the ratio of pure aPP, indicating that for this composition the surface may contain both components, with the majority component being *a*PP.

SFG spectra of high molecular weight *a*PP2, *a*EPR7, and a 50:50 wt % *a*PP2/*a*EPR7 blend are shown in Figure 7b. In this case, the spectra of the blend are also nearly identical to the spectra of *a*PP2, indicating preferential segregation of polypropylene at the monolayer level. The SFG CH_2:CH_3 mode strength ratio for *a*PP2 and for the 50:50 wt % *a*PP2/*a*EPR7 blend is plotted in Figure 8. The mode strength ratio for the blend strongly favors *a*PP2, suggesting that *a*PP2 covers the surface and that partial wetting of *a*PP is not an issue for the 50:50 wt % blend under the experimental conditions.

Surface Composition of the Top 6−8 nm of *a*PP, *a*EPR, and Blends. *XPS Spectra of Poly(ethylene-co-propylene) Rubber Series.* XPS has been used to integrate the composition of the top 6.1 ± 0.8 nm of the films. The *a*EPR series is used again as a calibration

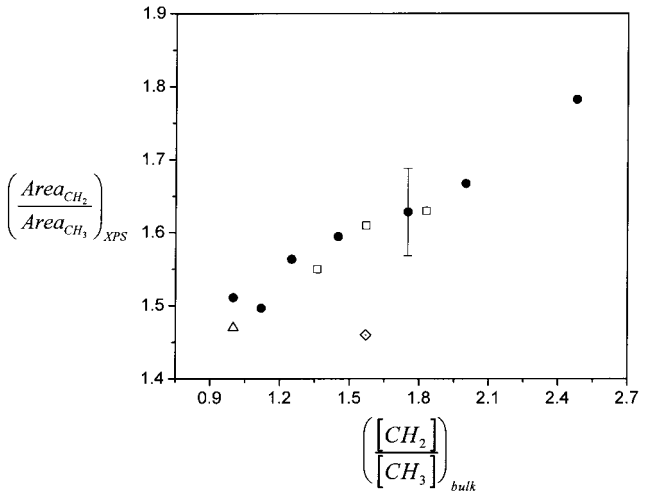

Figure 10. Valence XPS CH_2/CH_3 peak area ratio, ($Area_{15eV}$ + $Area_{21eV}$)/$Area_{18eV}$, vs bulk $[CH_2]/[CH_3]$ composition for *a*PP1 and the *a*EPR copolymers (●), *a*PP1/*a*EPR7 blends (□), *a*PP2 (△), and *a*PP2/*a*EPR7 blends (dotted ◇). The ratio for the aPP1/aEPR7 blends follows the ratio for the copolymers, indicating that top 6−8 nm of the blends contain significant quantities of both components. The ratio for the *a*PP2/*a*EPR7 blends is significantly enriched in CH_3, indicating that there is a layer of *a*PP2 at the surface which is at least 6.1 ± 0.8 nm thick.

set. XPS spectra of the carbon 1s core peak at 285 eV for *a*PP and *a*EPR are virtually identical. The valence band spectra, shown in Figure 9, however, show significant differences. Both polymers have peaks at 15 and 21 eV that are assigned to the 2s bonding and antibonding orbitals from the $-CH_2-$ backbone units of the polymers.[15] Both polymers have an additional feature at 18 eV that is two overlapping peaks, assigned to the 2s bonding and antibonding orbitals of the pendant CH_3 group. The broad feature at 9 eV arises from the carbon 2p band.

The valence band XPS spectra of *a*EPR7, which contains both ethylene and propylene monomers, has smaller CH_3 features relative to the CH_2 features compared to similar ratios in the valence band spectra of *a*PP. To quantify this result, after background subtraction, each *a*EPR valence band spectra has been fit to four peaks. The fitted spectra for *a*PP and *a*EPR7 are represented by the solid lines that are also presented in Figure 9. A plot of the ratio of the CH_2 fitted peak areas to the CH_3 fitted peak area as a function of the bulk $[CH_2]/[CH_3]$ ratio for the *a*EPR series (Figure 10) yields a linear relationship—consistent with the random nature of the *a*EPR copolymers. As the technique is sensitive to a much greater depth than SFG, it is insensitive to the orientation effects seen in the SFG data. The ratio of fitted peak areas is used here to characterize the relative methyl group concentration of the top few nanometers of the blend films.

Blend Systems. The CH_2/CH_3 XPS peak area ratios vs the bulk $[CH_2]/[CH_3]$ ratios for *a*EPR7 blends with low molecular weight *a*PP1 are shown in Figure 10 along with the ratios for the *a*EPR calibration series. The CH_2/CH_3 peak area ratio for each low molecular weight blend sample (33:67, 50:50, and 67:33 wt % *a*PP1/*a*EPR7) fits nearly identically to the peak area ratios for the copolymer series. This indicates that the *a*PP1 enrichment that is observable by SFG for this sample is not detectable at the level of resolution of XPS. Since the depth that the XPS is integrating over is estimated at 6.1 ± 0.8 nm, this indicates that the *a*PP1

Table 2. Summary of Bulk Phase Behavior Measured by DSC and Surface Compositions Measured by SFG and XPS for the 50:50 *a*PP1/*a*EPR7 System and the 50:50 *a*PP2/*a*EPR7 Blend Systems

bulk composition	DSC (bulk)	SFG (surface monolayer)	XPS (top 6.1 ± 0.8 nm)
50:50 aPP1/*a*EPR7	single phase	*a*PP1 enriched	mixed *a*PP1/*a*EPR7
50:50 *a*PP2/*a*EPR7	phase separated	*a*PP2 enriched	*a*PP2 enriched

enrichment layer is very thin—the top 5−7 nm contains significant quantities of each of the two components. Considering the sampling depth and the signal-to-noise of the measurement, it is likely that the highest levels of *a*PP in the surface enrichment layer are restricted to the top 2−3 nm of the film.

The *a*EPR7 blend system with high molecular weight *a*PP2 behaves quite differently. The CH_2/CH_3 peak area ratio for the 50:50 wt % blend is also shown in Figure 9. For this blend composition, the spectra show a significant depletion of the CH_2/CH_3 ratio relative to the bulk $[CH_2]/[CH_3]$ ratio. This indicates that the top 6.1 ± 0.8 nm of the high molecular weight blend is strongly enriched in *a*PP2.

Discussion

The bulk phase behaviors observed by DSC and the corresponding surface compositions observed by SFG and XPS for the two blend systems are summarized in Table 2. For both blend systems, *a*PP preferentially coats the surface at a monolayer level. The low molecular weight miscible blend (*a*PP1/*a*EPR7) has an enrichment layer less than ∼3 nm thick—beyond the resolution of our XPS experiment. The high molecular weight bulk immiscible system (*a*PP2/*a*EPR7) has a much thicker enrichment layer, which is detectable by XPS. The *minimum* thickness of this layer is ∼6.1 ± 0.8 nm.

The results of these experiments are qualitatively similar to the studies on surface segregation of blends of polyolefin copolymers with ethyl side branches and show another case where highly branched copolymers tend to segregate to the air/polymer surface.[1−3] The enrichment layer for the ethyl branched copolymers has been proposed to have its origins in the enthalpic cohesive energy. That is, polymer chains with higher branch ratios do not tend to pack as well as less branched chains and tend to have fewer interactions with other chains, leading to a low cohesive energy. By being at the surface, a highly branched chain loses fewer enthalpic interchain interactions than a less branched chain. It has also been argued that conformational entropy is an important consideration, with the component having the lower value of β^2 ($\beta^2 = R_g^2/V$; R_g is the radius of gyration and V is the chain volume) favored at the surface.[5] For most polyolefins, this also happens to be the more branched component.

Our results support the previous experimental evidence that a high density of side branches leads to enhanced surface activity. Additionally, the SFG results indicate that the orientation of the side branches at the surface may be an important factor in determining the surface activity. The *a*EPR copolymers have been shown to preferentially orient methyl groups out of the surface—consistent with theoretical predictions performed by Theodorou on atactic polypropylene.[25] This may mean that at least part of the surface segregation tendency of higher branched polymers may be due to specific interactions between the polymer and the low-density air interface which tend to maximize the number of bulky hydrophobic side branches extending out of the surface. Because *a*PP was ultimately shown by SFG to have a larger number density of methyl groups orienting away from the surface than *a*EPR,[13] *a*PP should be the more surface-active component on these grounds. For the air/polymer interface and the *a*PP/*a*EPR system, any segregation based on this effect would be working in parallel with the cohesive energy contributions as well as other conformational entropy contributions.

The SFG analysis presented in ref 13 also suggests that both *a*PP and *a*EPR7 polymer backbone segments at the interface are oriented parallel to the air interface and that *a*EPR7 assumes has longer chain segments at the surface than *a*PP. This result indicates that the ethylene-rich *a*EPR7 copolymer backbone packs better at the interface than the *a*PP backbone. This experimental evidence along with the SFG results for the *a*PP/*a*EPR7 blend suggests that the packing entropy contributions based on the orientation of the chain backbone at the interface do not significantly affect the surface segregation properties at the air/polymer interface. The packing entropy may an important factor at a high-density confined interface. Detailed experimental measurement of the *a*PP and *a*EPR7 chain configurations at the confined interface is the subject of ongoing investigations.

Comparison of Measured *a*PP Enrichment Layer Thickness with Theoretical Thickness Calculation. Models based on a Flory−Huggins energy of mixing, namely the Schmidt−Binder model and the exponential approximation to the Schmidt−Binder model, have recently been shown to give reliable results for modeling composition profiles of bulk miscible polymer blends with submicron thick surface enrichment layers.[2,4] Applying the exponential approximation model to the *a*PP1/*a*EPR7 system, it is assumed that the surface concentration of *a*PP1 ($\phi_{aPP,0}$) decays to the bulk concentration of *a*PP1, $\phi_{aPP1,\infty}$, through the exponential shown in eq 4 where z is the depth from the surface.

$$\phi_{aPP,z} = \phi_{aPP,\infty} + (\phi_{aPP,0} - \phi_{aPP,\infty})e^{(-z/\epsilon_b)} \qquad (4)$$

The decay length of the *a*PP enrichment, ϵ_{aPP}, is given by eq 5 and depends on the first two terms on the right-hand side which contain combinatorial contributions and the third term which contains contributions from specific pairwise interactions between *a*PP and *a*EPR7 characterized by the bulk interaction parameter, $\chi_{aPP/aEPR7}$, of the two components.

$$\epsilon_{aPP} = \frac{a}{6}\left[\frac{\phi_{aPP}}{2n_{aPP}} + \frac{\phi_{aEPR7}}{2n_{aEPR7}} - \chi_{aPP/aEPR7}\phi_{aPP}\phi_{aEPR7}\right]^{-1/2} \qquad (5)$$

In eq 5, a is the weighted statistical segment length of *a*PP and aEPR7, n_{aPP} and n_{aEPR7} are the degrees of polymerization for *a*PP and *a*EPR, ϕ_{aPP} is the volume fraction of *a*PP in the blend, and ϕ_{aEPR7} is the volume fraction of *a*EPR7. The decay length, ϵ, and thus the thickness of the enrichment layer are greater for high molecular weight blends (large n) and for blends that

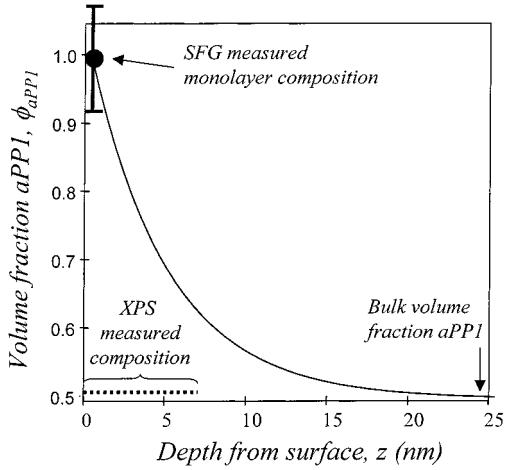

Figure 11. Comparison between experimentally measured surface compositions and the theoretical composition profile for the 50:50 wt % *a*PP1/*a*EPR7 bulk miscible blend: SFG measured composition (●); XPS measured composition (bracketed region)—the shading reflects the experimental error in the XPS measurement. Theoretical composition profile of 50:50 *a*PP1/*a*EPR7 based on eqs 4 and 5 (solid curve).

have a large interaction parameter, χ_{ab}. As discussed earlier, the 50:50 wt % *a*PP1/*a*EPR7 blend is miscible and should be amenable to treatment by eq 4 and eq 5, provided $\chi_{aPP/aEPR7}$ is known. The procedure used to estimate $\chi_{aPP/aEPR7}$ is given in the Appendix.

The compositional depth profile of the bulk miscible system estimated using eqs 4 and 5 with $\chi_{aPP/aEPR7}$ set to 0.001 02 and a value of 0.55 nm for *a*, the weighted segment length of *a*PP and aEPR7,[27] is shown in Figure 11. Since the SFG data showed that *a*PP1 completely coated the surface, the monolayer *a*PP1 composition (ϕ_0) was set at 1. The resulting curve in Figure 10 shows that the *a*PP1 enrichment at the uppermost monolayer (as measured by SFG) should decay to 90% of the bulk composition at a depth of 10 nm. This estimate is reasonable in the context of the XPS experiment. The XPS measured composition is shown by the bracketed region. The shaded region represents the error in the XPS measurement. Since XPS integrates over ~6−8 nm of the surface, the model predictions of a depletion of *a*EPR7 within the top 2−3 nm is likely outside the resolution of the XPS experiment.

The higher molecular weight *a*PP2/*a*EPR7 blend is bulk immiscible. For this case the *a*EPR7 depletion is observed by both SFG and XPS, indicating a much stronger enrichment of the *a*PP in the immiscible blend. This is consistent with literature thin film studies which show that equilibrium bilayers can develop in immiscible polymer blends with the surface active component (*a*PP) at the air−polymer interface.[2] This suggests the possibility of much larger penetration depths of *a*PP2 and is consistent with the observed enrichment of *a*PP2 by both SFG and XPS. Interestingly, we still observe nearly pure *a*PP2 by SFG in the immiscible blend (Figure 8) despite the fact that the DSC results in Figure 3c indicates some mixing of *a*EPR7 in the bulk *a*PP-rich phase (see Appendix). This indicates preferential wetting of *a*PP2 at the surface monolayer within the *a*PP-rich surface region.

Conclusion

The surface monolayer composition of miscible and immiscible blends of atactic polypropylene (*a*PP) with aspecific poly(ethylene-*co*-propylene) rubber (*a*EPR) was characterized by SFG and XPS. SFG showed that polypropylene homopolymer segregated to the air/polymer interface for all blend compositions studied—consistent with the high surface activity of branched copolymers.

X-ray photoelectron spectroscopy was used to estimate the thickness of the *a*PP enrichment layer. Low molecular weight *a*PP/*a*EPR blend systems, which were shown by DSC to be bulk miscible, have a surface enrichment layer which is not detectable by XPS. This places the maximum thickness of ~3 nm for the enrichment layer. In *a*PP/*a*EPR blend system with higher molecular weight *a*PP2, the blends were shown by DSC to be bulk immiscible, and a surface excess of *a*PP2 was detectable by XPS, placing a minimum thickness of 6.1 ± 0.8 nm for the excess layer. These results show that

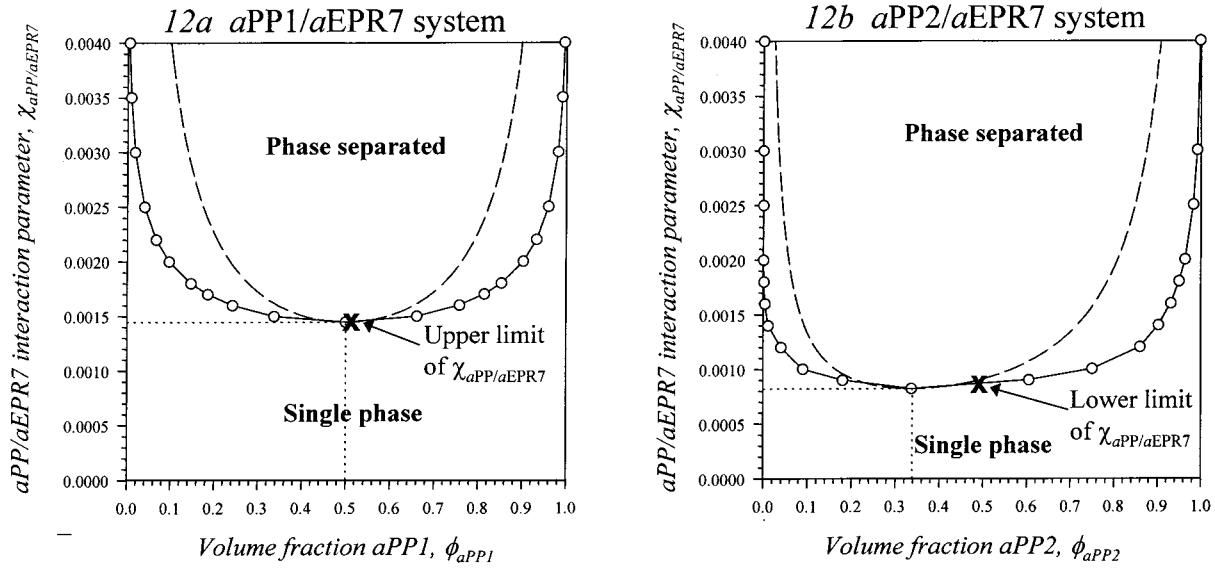

Figure 12. Calculated bulk phase diagrams for the blend systems (300 K): (a) Phase diagram for *a*PP1/*a*EPR7 blend system. Because DSC showed that the 50:50 wt % *a*PP1/*a*EPR7 blend was in a single phase, an upper limit of 0.00145 for $\chi_{aPP/aEPR7}$ can be established. (b) Phase diagram for the *a*PP2/*a*EPR7 blend system. Because the 50:50 wt % *a*PP2/*a*EPR7 blend was shown to be phase separated in the bulk, a lower limit of 0.00087 for $\chi_{aPP/aEPR7}$ can be established.

while differences in the surface activities of the individual components control the surface monolayer composition, the interaction parameter (χ_{ab}) and the bulk miscibility control the thickness of the surface enrichment layer.

Acknowledgment. This work was supported by the Director, Office of Science, Office of Basic Energy Sciences, Division of Materials Science and Engineering, of the U.S. Department of Energy under Contract No. DE-AC03-76SF00098 and by Basell Polyolefins. The authors acknowledge polymer synthetic assistance from Robert L. Jones and material characterization assistance from Debby Morgan, Alexander Marchione, Dr. Bill Long, and Dr. Robert Zeigler.

Appendix. Estimate of *a*PP/*a*EPR7 Interaction Parameter, $\chi_{aPP/aEPR7}$

Our estimate of the interaction parameter between *a*PP and *a*EPR7, $\chi_{aPP/aEPR7}$, is based on the DSC observation that the *a*PP1/*a*EPR7 blend is in a single bulk phase and that the *a*PP2/*a*EPR7 blend is phase separated in the bulk. Equation 6, the standard free energy of mixing from Flory−Huggins theory, is used as a first approximation to describe the *a*PP/*a*EPR7 blends. The first two terms on the right-hand side represent combinatorial contributions to the mixing energy, and the third term represents contributions from specific pairwise interactions between *a*PP and *a*EPR7.

$$\frac{\Delta G}{RT} = \frac{\phi_{aPP}}{n_{aPP}v_{aPP}/v_0}\ln(\phi_{aPP}) + \frac{\phi_{aEPR7}}{n_{aEPR7}v_{aEPR7}/v_0}\ln(\phi_{aEPR7}) + \phi_{aPP}\phi_{aEPR7}\chi_{aPP/aEPR7} \quad (6)$$

In eq 6, ΔG is the molar free energy of mixing, $\phi_{aPP,aEPR7}$ are the volume fractions of *a*PP and *a*EPR7 in the blend, $v_{aPP,aEPR}$ are the molar volumes of *a*PP and *a*EPR, v_0 is a reference volume (taken as $v_0 = (v_{aPP}v_{aEPR7})^{1/2}$), and $n_{aPP,aEPR7}$ are the degrees of polymerization of the two polymers. Evaluation of the binodal, spinodal, and critical conditions for binary mixtures followed standard procedures, and the results are given in parts a and b of Figure 12 for the *a*PP1/*a*EPR7 and *a*PP2/*a*EPR7 blends, respectively, as a function of the interaction parameter, $\chi_{aPP/aEPR7}$.[28] The critical composition ($\phi_{aPP,c}$), the blend composition with the highest tendency to phase separate and the corresponding critical value of the interaction parameter, χ_c, are given by

$$\phi_{aPP,c} = \frac{(n_{aEPR7}v_{aEPR7}/v_0)^{1/2}}{(n_{aPP}v_{aPP}/v_0)^{1/2} + (n_{aEPR7}v_{aEPR7}/v_0)^{1/2}} \quad (7)$$

$$\chi_c = \frac{\{(n_{aPP}v_{aPP}/v_0)^{1/2} + (n_{aEPR7}v_{aEPR7}/v_0)^{1/2}\}^2}{2(n_{aPP}v_{aPP}/v_0)(n_{aEPR7}v_{aEPR7}/v_0)} \quad (8)$$

Based on eqs 7 and 8, $\phi_{aPP,c}$ and χ_c are calculated to be 0.500 and 0.00145, respectively, for the *a*PP1/*a*EPR7 blend and 0.3366 and 0.000821, respectively, for the unbalanced molecular weight *a*PP2/*a*EPR7 blend. The critical conditions are marked by dotted lines in Figure 12a,b. From Figure 12a, the value of $\chi_{aPP/aEPR7}$ which would lead to phase separation of the 50:50 wt % *a*PP1/*a*EPR7 blend is evaluated to be 0.00145. Because this blend is *miscible* by DSC, it follows that 0.00145 is a maximum value of $\chi_{aPP/aEPR7}$. From Figure 12b, the value of $\chi_{aPP/aEPR7}$ which would lead to phase separation of the 50:50 wt % *a*PP2/*a*EPR7 blend is evaluated to be 0.00087. Because this blend is *immiscible* by DSC, it follows that 0.00087 is the miminum value of $\chi_{aPP/aEPR7}$.

We can further estimate $\chi_{aPP/aEPR7}$ by noting that the glass transition temperatures of the immiscible blend in Figure 3c are shifted relative to the pure components. The T_g of the *a*EPR7-rich phase is −43.0 °C relative to −46.2 °C for the pure *a*EPR7 component. Similarly, the T_g of the *a*PP2-rich phase is −10.6 °C relative to +0.2 °C for the pure *a*PP2 pure component. Mixing of the minority component in both phases causes an elevation of the T_g for the *a*EPR7-rich phase and a decrease of the T_g for the *a*PP2-rich phase. These values of the glass transition temperature vary by only a few degrees with casting solvent and after a reheat in the DSC, so it is felt that they represent a reasonable approximation to the binodal compositions in the 50:50 wt % *a*PP2/*a*EPR7 blend.

For the individual copolymers and the miscible *a*PP1/*a*EPR7 blend, the Gordon−Taylor correlation described very well the composition dependence on the glass transition temperature.[29] Using this correlation, the compositional changes associated with the observed glass transition shifts in the 50:50 wt % *a*PP2/*a*EPR7 blend could be estimated, and the associated $\chi_{app/aEPR7}$ is calculated from Figure 11b to be 0.00102 ± 0.00010 (the error reflects the different result calculated from the *a*EPR7-rich and *a*PP2-rich portions of the phase diagram) without any further correction for temperature. This assignment also predicts that the *a*PP-rich phase is the dominant component relative to the *a*EPR7-rich phase in roughly a 60:40 ratio, which is in qualitative agreement with the smaller heat capacity change observed for the *a*EPR7-rich phase in Figure 3c.

References and Notes

(1) Scheffold, F.; Budkowski, A.; Steiner, U.; Eiser, E.; Klein, J.; Fetters, L. J. *J. Chem. Phys.* **1996**, *104*, 8795.
(2) Klein, J.; Kerle, T.; Zink, F.; Eiser, E. *Macromolecules* **2000**, *33*, 1298.
(3) Budkowski, A.; Rysz, J.; Scheffold, F.; Klein, J.; Fetters, L. J. *J. Polym. Sci., Part B: Polym. Phys.* **1998**, *36*, 2691.
(4) Schmidt, I.; Binder, K. *J. Phys. (Paris)* **1985**, *46*, 1631.
(5) Wu, D. T.; Fredrickson, G. H. *Macromolecules* **1996**, *29*, 7919.
(6) Donley, J. P.; Wu, D. T.; Fredrickson, G. H. *Macromolecules* **1997**, *30*, 2167.
(7) Kokkinos, I. G.; Kosmas, M. K. *Macromolecules* **1997**, *30*, 577.
(8) Zink, F.; Kerle, T.; Klein, J. *Macromolecules* **1998**, *31*, 417.
(9) Zhao, X.; Zhao, W.; Sokolov, J.; Rafailovich, M. H.; Schwarz, S. A.; Wilkens, B. J.; Jones, R. A. L.; Kramer, E. J. *Macromolecules* **1991**, *24*, 5991.
(10) Jones, R. A. L.; Kramer, E. J.; Rafailovich, M. H.; Sokolov, J.; Schwartz, S. A. *Phys. Rev. Lett.* **1989**, *62*, 280.
(11) Zhang, D.; Shen, Y. R.; Somorjai, G. A. *Chem. Phys. Lett.* **1997**, *281*, 394.
(12) Gracias, D. H.; Zhang, D.; Lianos, L.; Ibach, W.; Shen, Y. R.; Somorjai, G. A. *Chem. Phys.* **1999**, *245*, 277.
(13) Opdahl, A.; Phillips, R. A.; Somorjai, G. A., *J. Phys. Chem. B*, in press.
(14) Jones, R. A. L. *Polymer* **1994**, *35*, 2160.
(15) Galuska, A. A.; Halverson, D. E. *Surf. Interface Anal.* **1998**, *26*, 425.
(16) Resconi, L.; Jones, R. L.; Rheingold, A. L.; Yap, G. P. *Organometallics* **1996**, *15*, 998.
(17) Koenig, J. L. *Chemical Microstructure of Polymer Chains*; John Wiley & Sons: New York, 1982.
(18) Wei, X.; Hong, S. C.; Zhuang, X. W.; Goto, T.; Shen, Y. R. *Phys. Rev. E* **2000**, *62*, 5160.
(19) Miranda, P. B.; Shen, Y. R. *J. Phys. Chem. B* **1999**, *103*, 3292.

(20) Roberts, R. F.; Allara, D. L.; Pryde, C. A.; Buchanan, D. N. E.; Hobbins, N. D. *Surf. Interface Anal.* **1980**, *2*, 5.
(21) Briggs, D. *Surface Analysis of Polymers by XPS and Static SIMS*; Cambridge University Press: New York, 1998; Chapter 2.2, pp 27−46.
(22) Briggman, K. A.; Stephenson, J. C.; Wallace, W. E.; Richter, L. J. *J. Phys. Chem. B* **2001**, *105*, 2785.
(23) Wang, J.; Chen, C. Y.; Buck, S. M.; Chen, Z. *J. Phys. Chem. B* **2001**, *105*, 12118.
(24) Oh-e, M.; Lvovsky, A. I.; Wei, X.; Shen, Y. R. *J. Chem. Phys.* **2000**, *113*, 8827.
(25) Mansfield, K. F.; Theodorou, D. N. *Macromolecules* **1990**, *23*, 4430.
(26) Clancy, T. C.; Jang, J. H.; Dhinojwala, A.; Mattice, W. L. *J. Phys. Chem. B* **2001**, *105*, 11493.
(27) Segment length is defined here as $a = R_{g,w}/(N_w/6)^{1/2}$ where $R_{g,w}$ is the radius of gyration and N_w is the degree of polymerization. The weighting of component a values in the blend is according to ref 8.
(28) Strobl, G. *The Physics of Polymers*; Springer-Verlag: Berlin, 1996.
(29) Gordon, M.; Taylor, J. S. *J. Appl. Chem.* **1952**, *2*, 493. Wood, L. A. *J. Polym. Sci.* **1958**, *28*, 319.

MA011773Q